Conceptual design of a liquid-metal divertor for the European DEMO

Fusion Engineering and Design 173 (2021) 112812

Contents lists available at ScienceDirect

Fusion Engineering and Design

journal homepage: www.elsevier.com/locate/fusengdes

Conceptual design of a liquid-metal divertor for the European DEMO

P. Rindt [*,a], J.L. van den Eijnden [a], T.W. Morgan [a,b], N.J. Lopes Cardozo [a]

[a] Eindhoven University of Technology, De Zaale, Eindhoven 5612AZ, The Netherlands
[b] DIFFER - Dutch Institute For Fundamental Energy Research, De Zaale 20, Eindhoven 5612AJ, The Netherlands

ARTICLE INFO

Keywords:
DEMO
Liquid metal
Divertor

ABSTRACT

Liquid metal (LM) divertors are considered for the European DEMO reactor, because they may offer improved performance compared to the tungsten monoblock concept. The goal of this work is to provide a concept design, and explore the limitations of liquid metal divertors. To this end, a set of design requirements was formulated in close collaboration with the EUROfusion Power Plant Physics and Technology team (responsible for the design of the EU-DEMO). Tin was chosen as the preferred liquid metal, because unacceptable Tritium retention issues arise when lithium is used in DEMO. A concept design was then chosen that consists of water cooled pipes that are square on the outside and round on the inside, a corrosion barrier, and a 3D-printed porous tungsten armor layer filled with liquid tin. The porous armor layer acts as a Capillary Porous System (CPS). The design was analyzed using thermo-mechanical FEM simulations for various armor thicknesses and heat sink materials: Densimet, W/Cu composites, and CuCrZr. The highest heat loading capability achieved is 26.5 MW/m^2 in steady state (18.9 MW/m^2 when taking into account a safety margin of 1.4). This is achieved using a CuCrZr pipe, with a 1.9 mm thick armor. When increasing the armor layer to 3 mm thick, more than 80 MW/m^2 can be withstood during slow transients thanks to vapor shielding, but at the same time the steady-state capability is reduced to 18 MW/m^2. Resilience against disruptions cannot yet be proven, but is deemed within the realm of possibility based on estimates regarding the behavior of vapor shielding. This should be further investigated. Overall, the concept is considered a significant improvement compared to the original specifications (which are also the specifications to the tungsten monoblocks: 10 MW/m^2 in steady state, and $\sim$ 20 MW/m^2 during slow transients). Moreover, the possibility of withstanding disruptions is regarded as a potentially major improvement.

1. Introduction

To deliver a high performance fusion power plant, liquid metal-based divertors (LMDs) present a promising option compared to solid (W) based divertors such as the DEMO baseline ITER-like design [1,2]. LMDs feature improved robustness against transient loading (e.g. disruptions), which is achieved via vapor shielding. Additionally because the component can be thinner than the baseline design due to the self-replenishing liquid surface, it is possible to increase the tolerable steady-state heat loads. In such a case reactors can be designed to be smaller [3], and thus more economical. An example of this approach is the ARC tokamak, which aims at delivering the same fusion power as ITER (500 MW) in a device with half the major radius (3.3 m compared to 6.2 m) [4]. In this work, we focus on the design of an LMD for the nearest step towards a fusion power plant: the European DEMO.

The EU-DEMO reactor completed the pre-conceptual design stage in 2020 [5], and aims to complete the conceptual design phase in 2027. To incorporate an LMD in the EU-DEMO, a viable engineering concept should be developed on a similar timescale. In spite of this, LMD designs are not yet at a sufficient technological readiness level. Solid tungsten divertors are already developed further within the EUROfusion DIV work package. They are undergoing extensive testing and analysis [6–8], which can be taken as an example. For LMDs, a concept should first be developed for testing at intermediate stages such as a Divertor Test Tokamak, DTT. Presently, concept designs are needed with the potential to fulfill the requirements for DEMO, that can eventually be tested as thoroughly as the solid divertors.

This work was supported by a EUROfusion engineering grant and performed in close collaboration with the Power Plant Physics and Technology (PPPT) team (which is responsible the design of the EU-DEMO), and in collaboration with the EUROfusion DIV and LMD work packages (which are responsible for the design of the tungsten

* Corresponding author.
E-mail address: prindt@gmail.com (P. Rindt).

https://doi.org/10.1016/j.fusengdes.2021.112812
Received 23 April 2021; Received in revised form 13 July 2021; Accepted 27 July 2021
Available online 7 August 2021

monoblock concept, and the liquid metal divertor concepts respectively). Asides from the concept described in this work, other LMD concepts are under development as well within the work package LMD, a first description of which can be found in [9].

Existing designs of liquid metal components are considered in the design process. There are important lessons to be learned from these, even though none of these can be directly applied in their current form. The most important are: First, the theory describing LM surface stability [10], and the effective suppression of LM splashing by using capillary porous systems (CPS) [11–13]; second, the theory and practical demonstration of vapor shielding, which provide an estimate of power handling capability and LM surface temperatures [14–18]; third, the concept of a vapor box, which can be used to prevent excessive LM concentrations in the core plasma, despite high evaporation rates [19]; and fourth, the studies of LM flow to dissipate heat through convection [20,21], which indicate the importance of $J \times B$ driven forces and MHD drag. Related to the design requirements, also the studies regarding the LM loss rate and plasma contamination are crucial [22–24]. Namely these studies provide concrete limits for allowable LM evaporation rates.

The approach of this work is to design a concept from the ground up, in order not to be hindered by assumptions that may not be valid for the EU-DEMO. In Section 2, first the design requirements for DEMO are formulated. Next, a concept is chosen and developed into a more detailed concept design. This design is presented in Section 4, and its heat loading capability is analyzed in Section 5. The exact design of the porous structure in which the liquid metal will be confined is discussed in Section 6. Finally, in Section 7 it is assessed whether the design meets all requirements for the EU-DEMO, and also the potential for further improvement is discussed.

2. Design requirements

The main functionality of the divertor target is that of the power exhaust. The divertor must therefore be resistant against the power flux from the plasma, and given its location, it must also be resistant against various other loads. These include the neutron flux and resulting decay heat (~3 W/cm^3 [25]), and EM-forces created by halo currents during disruptions and Vertical Displacement Events (which can be up to 272 kA in a single divertor cassette [25]). Furthermore, machine compatibility requirements must be satisfied. For example, the targets must fit within the available space. The following requirements were found to be the most relevant to the concept design proposed here. References are given where possible. In other cases requirements are based on internal decisions made within the PPPT team.

1. **In normal steady-state operation, the local maximum heat flux of 10 MW/m^2 must be tolerated, and up to 17 to 21 MW/m^2 during slow transients of 3 to 10 seconds** [1]. **Outside the strike point the load will be kept below 5 MW/m^2.**
2. **During disruptions, the load on the divertor can peak at 80 GW/m^2. The total length of the pulse is about 4 ms** [26]. Such an event must be withstood at least one time throughout the lifetime of the divertor.
3. **The design must take into account a safety margin of 40% for the tolerable heat flux density.**
4. **The lifetime of the LMD must be at least 2 full power years (FPY).**
5. **The design of the tritium fuel cycle for DEMO, and the tritium inventories, may not require significant changes for the sake of the LMD.** This requirement is imposed because the availability of tritium, and its efficient use, are critical constraints for the viability of a reactor [27–30]. The design of the fuel cycle, and the systems involved are therefore leading.
6. **The LM must not significantly reduce core plasma performance.** The work from [22] estimates net loss rates based on literature, and provides an estimate for the maximum strike point temperature, which is 1250 °C for tin, and 690 °C for lithium.
7. **The divertor must be a high recycling surface.** The physics basis for DEMO is based on the most relevant experiment available: ITER. In ITER, it is assumed that the divertor will be a high recycling surface.
8. **Activation should be kept below the allowable limits for low or intermediate level nuclear waste.** This results in a maximum usage of elements, presented in [31].
9. **The divertor target must be 70 cm wide, and it must be oriented near vertically.** This width of the target is required due to the uncertainty in the strike point location.
10. **It must be possible to re-wet the target, without removing the divertor cassette.** This guarantees that the target can continue to operate in case of accidental drying of the target, while minimizing the time required for maintenance.
11. **The divertor should withstand exposure to atmosphere for about 2 months during regular maintenance, and a 48 hour bake at 200 °C during subsequent start-up procedures.**
12. **The LM divertor must not require major design changes to diagnostic systems, or other in vessel components, including the first wall** This is required to maintain a manageable concept design phase for DEMO as a whole. However, in case significant improvements can be made that do require major changes to other systems, it should be considered if these changes can be realistically achieved.

Note that the use of LM will bring increased complexity to the divertor. Hence, to be worth its cost, a LMD must perform significantly better than its solid counterpart. Additionally, it is important to realize that the heat flux requirements presented here are not set by the plasma output power, but rather by the technological limit for the power handling capacity of a solid divertor. As such, the specified loads are simultaneously a requirement for actively controlled detachment control, which is responsible for heat load mitigation. In the case where accidental full re-attachment of the plasma occurs, the heat load can reach up to ~ 80 MW/m^2, far above the specified load (F. Maviglia and J.-H You, private communications). The capability to withstand such loads, or unmitigated ELMs and disruptions, can justify the use of LMDs.

Lastly, in DEMO, it is not required to use the power impinging on the divertor for electrical power generation. I.e. no minimum divertor coolant temperature is required for efficiency of the power plant steam cycle. Being able to use higher coolant temperatures than the monoblocks (150 °C, [2]) is, however, considered a benefit.

3. Liquid metal choice

The liquid metal species is the single most important parameter for the resulting concept design. This choice could be made independent of any other concept choice, and is therefore presented here first. The main candidates are lithium and tin (or an alloy the two). Out of these two, the authors regard tin as the most realistic for DEMO. The main reasons are that in DEMO, the use of lithium leads to issues with tritium retention as well as maintenance.

With regards to retention: Lithium has the potential to retain up to 100% of the incoming D/T [32], which is on the order of 10^{24} s^{-1}. To build a feasible reactor, the retained tritium must be separated from the lithium quickly enough to keep T inventory levels below the allowed limits, or, retention must be prevented in the first place. Filtering out the tritium is likely a significant challenge because the 100% retention of the incoming particle flux requires an order of magnitude higher throughput of the filtering system than currently foreseen for DEMO [30]. Moreover, this will require a complete overhaul of the DEMO fuel cycle, which highly undesirable (design requirement 5).

Preventing tritium retention is equally problematic. This can only be done by ensuring that any location that lithium can reach, is hot enough

to prevent the formation of LiD/T. The problems with this approach are, first, that strongly cooled components are required in DEMO. For example, port limiters for protection against disruptions [33,34]. Second, lithium can migrate through gaps in the wall armor and condense in colder areas behind it. Third, it is not certain if the strike point itself can be operated at a temperature where LiD/T formation is prevented, while maintaining an evaporation rate within the acceptable range [35]. The most fundamental issue is, however, that evaporated Li must inevitably be pumped or condensed somewhere, and D/T retention will be problematic in exactly these places.

With regards to maintenance: The maintenance periods require that the reactor can be under atmosphere for about two months (design requirement 11). During this period lithium surfaces will oxidize, and cause a safety hazard. Though no quantitative analysis has been carried out into the degree of oxidation, it is likely that a lithium divertor will need some form of protection against exposure to atmosphere, which is not straightforward.

For tin, current research suggests that tritium retention is comparable to tungsten [36–38], and therefore a problematic buildup of tritium inventory should not occur (however, further research on this topic is recommended). Moreover, exposure to atmosphere at room temperatures does not result in problematic oxidation, or safety hazards. For these reasons, tin is considered the most realistic LM choice for DEMO. It should be noted though that alloying or mixing with other elements is still possible as long as retention is prevented, and might be used to improve the material properties.

Finally, it should be noted that tin activates slightly. According to [31], no more than 10% of the entire first wall should be made up of Sn. Given that the divertor target area makes up only $\sim 8\%$ of the total surface area of the reactor, and the fact that only a few mm thick layers of Sn will be used, this should not be problematic.

4. Resulting concept design

4.1. Concept layout and working principles

The resulting concept is shown in Fig. 1. The incoming heat flux is conducted to a coolant through a layer of armor and the wall of the coolant channel. This is the same working principle employed in the monoblock design. However, here the armor consists of a Sn filled CPS on top of the coolant channel. This concept is chosen because both water cooling and the use of CPS are relatively well developed technologies. Pressurized water cooling has been applied successfully in nuclear fission plants, and in the monoblock designs for ITER and the EU-DEMO [2,39]. The capillary porous system is currently the most reliable method in the field to replenish a LM surface, and keep it stable against droplet ejection. Despite relying on the same working principle as the monoblock design, the power handling capability can be improved because the armor layer can be made much thinner. To supply sufficient Sn to the strike point, an array of pipes is placed inside a shallow bath. As required, this bath is oriented vertically. Because the required height of 700 mm is too high to create a static liquid column held up by capillary forces, the flow scheme from Fig. 2 is applied. Tin is injected at the top of the component, and flows down due to gravity. At the bottom it is collected and pumped back up. Heating of the Sn in this loop should be considered in future detailed design activities, to ensure that the Sn remains liquid and can indeed be pumped, but this may not be necessary due to the high temperature environment. The parameters that determine the tolerable heat load for this design are the width w of the pipe, the diameter D of the coolant channel, the thickness t of the armor, the pipe and armor material choice, and the coolant pressure P, bulk temperature T_b, and velocity v.

The coolant channel is round to avoid high stresses in the pipe due to the coolant pressure. On the other hand, the pipe is square on the outside to ensure as homogeneous cooling as possible for the PFS. The width of the pipe and diameter of the channel are set to $w = 10$ mm and $D = 8$

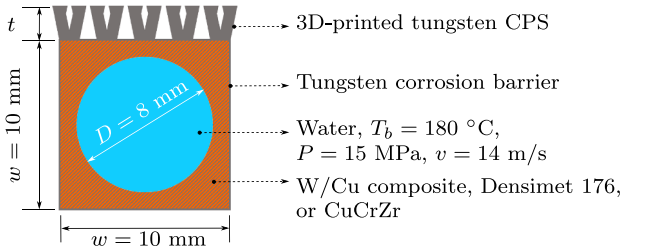

Fig. 1. Concept chosen for DEMO: Similar to a monoblock, the incoming heat flux is directly conducted to a coolant. Under the strike point the Sn surface temperature can be kept sufficiently low due to the low thickness of the CPS. Yet, during slow transients, vapor shielding will become relevant before the coolant boils excessively. Water at 180 °C is used so that sufficient heat flux density can be tolerated before the CHF is reached, while keeping the top layer of Sn liquid in regions with lower heat flux density.

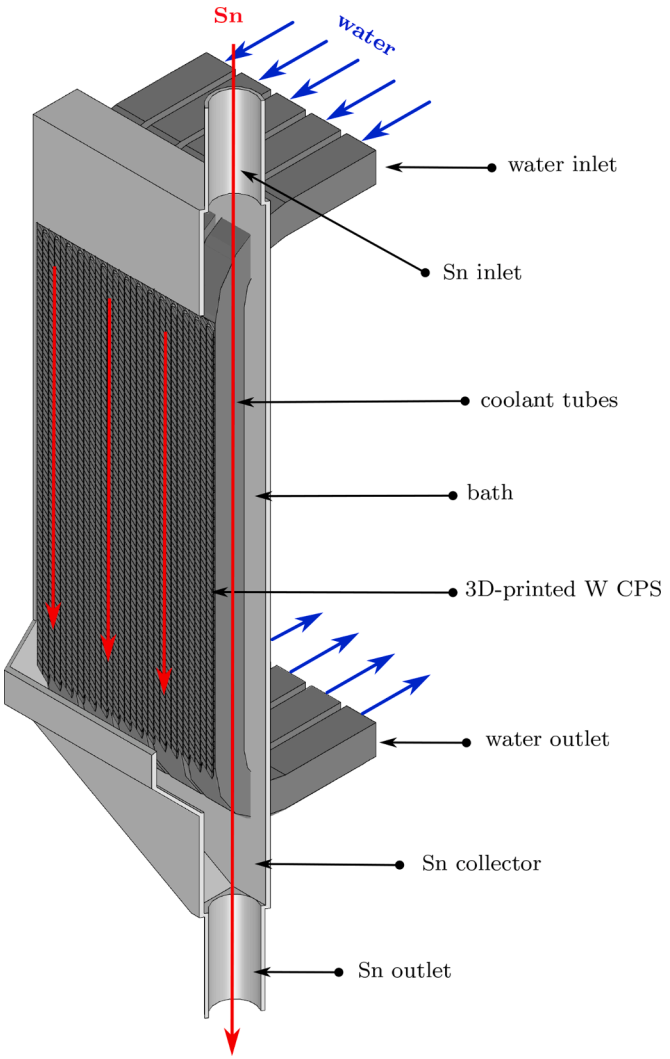

Fig. 2. Impression of a full divertor target assembly. The coolant channels and Sn filled CPS are constructed as shown in Fig. 1. An array of pipes is placed in a shallow bath, which is fed with tin from the top, and drained from the bottom. In combination with the 3D-printed CPS, this strategy can be used to optimize the LM re-supply rate to the strike point. In case of unexpected dry-out, this system can also be used to force re-wetting by increasing the Sn flow.

mm. The armor thickness t must be on the order of 1 to 3 mm. It must be thin enough to keep evaporation with the acceptable range during steady state operation, but, meanwhile, the PFS must get hot enough to benefit from vapor shielding during slow transients. The influence of the thickness on the heat loading capability is investigated in Section 5. The armor thickness and material choices also influence the heat flux concentration factor (ratio of the heat flux density through the pipe inner wall to the heat flux density through the PFS). Because the LMD has a relatively smaller plasma facing surface area per cooling channel, this ratio is smaller than it is in the monoblocks (<1.35 compared to 1.6 in the DEMO monoblocks [2]).

4.2. CPS material and manufacturing

With regards to the CPS: tungsten is used because it has sufficient thermal conductivity, it is compatible with the nuclear environment, and it is resistant against corrosion by the tin [40]. The candidate pipe materials are not expected to be resistant to corrosion by tin, and will therefore also be cladded in a tungsten corrosion barrier. The CPS will be 3D-printed, which has the advantage that the internal structure can be optimized for the most beneficial flow and lowest thermal stresses. A detailed design of this structure is presented in Section 6. A second advantage of 3D-printing is that the resulting plasma facing surface is mechanically stable, provided a reliable joint between the CPS and the tungsten coated cooling channel can be made.

4.3. Coolant conditions

Because the incoming heat flux is conducted though the cooling pipes to the coolant, a coolant must be selected that can absorb high heat flux densities. Moreover, to keep the PFS temperature below the maximum of 1250°C a high convective heat transfer coefficient h is required. Finally, the coolant must have high enough temperature to keep the liquid metal liquid outside the strike point, where the background heat load is around 2.5 MW/m^2, from F. Maviglia, private communications and [25]. Water is selected as the most suitable candidate to meet these requirements.

The exact water pressure (P), bulk temperature (T_b), and flow velocity (v) must be chosen carefully. These determine the pipe wall temperature at which the water starts boiling (the onset of nucleate boiling, the convective heat transfer coefficient, and the critical heat flux density (CHF) beyond which all cooling capacity is lost due to excessive boiling. The behavior of these parameters is shown in Fig. 3 and 4. To maximize the critical heat flux, first the water pressure is set at 15 MPa. Increasing the pressure further does not increase the CHF. Next, the bulk temperature is set to 180 °C, which is the minimum temperature required to prevent solidification of the top millimeter of tin outside the strike point. The velocity is set to 14 m/s. Further increase has a negligible effect on the CHF and h.

Water under the selected conditions provides $h \approx 175$ kW/m^{2}K. Moreover, h increases when the wall temperature rises to the point where nucleate boiling starts, thus keeping the wall temperature almost constant. Note that nucleate boiling cannot be used in steady state operation, due to the erosion of the pipe material caused by the collapse of the bubbles. Under the selected conditions nucleate boiling starts when the pipe inner wall reaches 345 °C. The CHF through the inner wall is 56.1 MW/m^2. These calculations are based on a modified Sieder/Tate correlation and a Thom correlation [42] and [41].

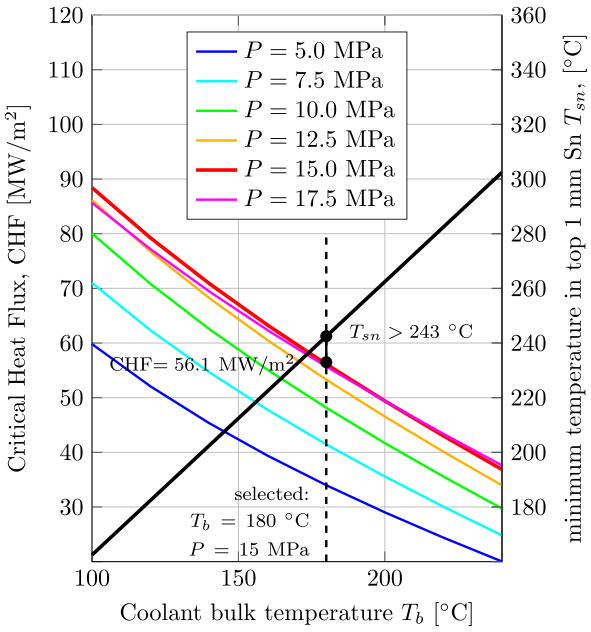

Fig. 3. Trade-Off in the choice for coolant bulk temperature T_b. Lower T_b allows for increased CHF (colored, left axis), but will eventually reduce the tin temperature (black, right axis) outside the strike point below the melting point (dashed). The CHF is calculated at various pressures using the modified Tong correlation from [41]. The minimum temperature in the top 1 mm of Sn is calculated assuming $h = 175$ kW/m^{2}K and an incoming heat flux density of 2.5 MW/m^2.

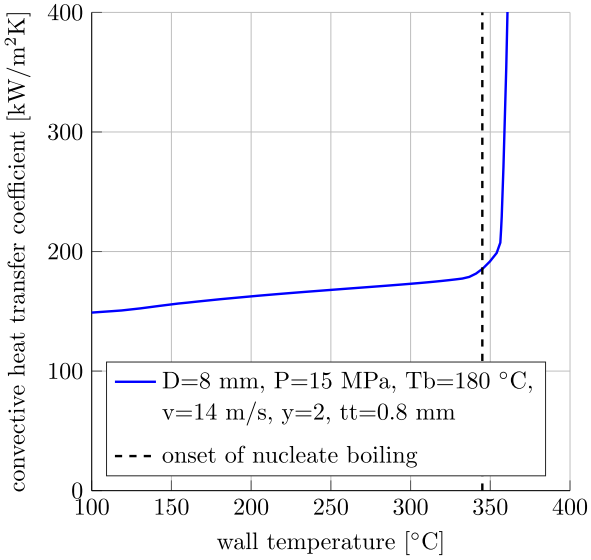

Fig. 4. Calculation of the convective heat transfer coefficient. A modified Sieder/Tate correlation is used before the onset of nucleate boiling, in the forced confection regime. Beyond this point a CEA/Thom correlation is used. Both are taken from [42] and [41].

5. Material candidates and performance analysis

5.1. Material candidates

The material used for the cooling pipes must have high thermal conductivity, and sufficient strength at high temperature. Several candidates are considered: copper chrome zirconium alloy (CuCrZr) [43,44], W/Cu composite with 60 wt% tungsten [45,46], W/Cu composite with 85 wt% tungsten from [45,46], and Densimet grade 176 from Plansee [47,48]. Densimet is a composite of ~ 93% tungsten, with an iron and nickel binder. The advantage of this material and the other W/Cu composites is increased strength and reduced copper content (the latter reduces nuclear waste). The disadvantage is reduced thermal conductivity. The presence of nickel in Densimet is problematic in the nuclear environment, but this material is considered an interesting

proxy to assess the potential of composites with high tungsten content.

5.2. FEM model

The heat loading capability of the design is investigated using a thermomechanical model in COMSOL. An overview of the model geometry and applied boundary conditions can be seen in Fig. 5. The tungsten CPS is set to have a void fraction 62%, which is filled with tin. This is based on the CPS design presented in Section 6. The CPS is assumed not to have an influence on the thermal stresses in the pipe, and is neglected in the stress analysis. The pipe itself is constrained stress free. The thickness of the CPS is a variable. The incoming heat flux is modeled as a gaussian beam with a FWHM of 44 mm, on top of a homogeneous background load of 2.5 MW/m^2 [25]. Values of the power flux density mentioned in this analysis refer to the maximum value of the sum of both. Vapor shielding is implemented according to the model from [16]. In the steady state analysis a redeposition coefficient for eroded LM of $R = 0.99$ is used, and the dissipated energy per LM particle is assumed to be $\epsilon_{cool} = 1000$ eV. The latter is the order of magnitude obtained when the cooling function L_z from [23] is multiplied with an electron density of 10^{20} m^{-3} and a particle lifetime of 10^{-5} s. The behavior of the target during normal and off-normal operation are both modeled assuming a steady-state, because it is assumed that thermal equilibrium is reached during slow transients. A time dependent simulation is used to assess the behavior during millisecond transients.

5.3. Heat loading capability in steady state and slow transients

The main results from the analysis are summarized in Table 1 and 2, and it is immediately clear that the required steady-state heat flux density of 10 MW/m^2 is achieved for all considered pipe materials and CPS-thicknesses. The analysis using the FEM proceeded as follows: The maximum tolerable power in steady state is found when one of the following limits is encountered: First, the pipe inner wall must remain below the onset of nuclear boiling at 345°C; Second, the Sn surface must remain below 1250°C; Third, the pipe stress must remain below the yield stress. The maximum tolerable power during off-normal operation (slow transients) is also determined. In this case the heat flux through the pipe inner wall must remain below the CHF of 56.1 MW/m^2, and also the pipe stress must remain below the yield stress. Fig. 7 shows a typical thermal response under various loads. These temperatures are measured along the z-coordinate in the center of the pipe and along the side of the pipe, see fig. 5. Fig. 6 shows a typical result for the stress relative to the Von Mises stress.

The influence of the pipe material choice is investigated first, by finding the maximum steady state load for each case. This maximum is determined only by the limit on pipe inner wall temperature, and the limit on the stress. When the maximum heat flux density is found, the CPS thickness is set so that the PFS reaches the limit of ~1250 °C. At this temperature, vapor shielding plays a negligible role. From the results, it appears that the materials with the highest thermal conductivity can handle the highest heat load. Densimet 176 and the W/Cu 85/15 composite have higher strength, but they are still limited by the induced thermal stresses. This is due to their low conductivity, and subsequently higher temperatures at the top of the pipe. These temperatures increase thermal expansion and thermal stress, while reducing the local yield strength. The more conductive materials are not limited because of high thermal stresses, but rather because the coolant reaches the onset of nucleate boiling. CuCrZr, shows the best performance because it has the highest thermal conductivity, and roughly the same strength as the W/Cu 60/40 composite.

The influence of the armor thickness becomes clear when both steady-state operation and slow transients are considered. It appears that the maximum tolerable load during slow transients increases strongly with CPS thickness, while the tolerable load in steady-state decreases with a thicker CPS. The increased thickness makes the PFS reach higher temperatures for the same load, which results in more vapor shielded power and less power conducted to the cooling water. In the most extreme case of a 3mm thick CPS, more than 80 MW/m^2 can be withstood when using a CuCrZr heat sink. During slow transients, excessive Sn evaporation is not considered as a concern, because they are off-normal events. Hypothetically, high Sn evaporation rates could even contaminate the core and reduce the fusion power output, thus creating a feedback mechanism protecting the divertor. In steady-state operation, however, the evaporation is of concern, and the PFS temperature becomes the limiting factor. Thus, the maximum tolerable power in steady state decreases with thicker CPS layers. Depending on the overall reactor design, a balance between steady-state performance and resistance to slow transients can be found by varying the CPS thickness.

In conclusion, all considered materials and CPS thicknesses can withstand the required 10 MW/m^2. Densimet and W/Cu 85/15 can withstand the lowest heat flux densities of 15 and 22.5 MW/m^2 respectively. These materials are limited by the thermal stresses, and consequently cannot tolerate any higher loads during short transients. When pipes are made from W/Cu 60/40 or CuCrZr the steady state operation is limited by the onset of nucleate boiling in the cooling water, at 25.3 and 26.3 MW/m^2 respectively. But, during slow transients nucleate boiling is allowed, and higher heat flux densities are possible. Short transients in excess of 80 MW/m^2 can be withstood when a CPS of 3mm is applied onto a CuCrZr heat sink.

Table 1
Maximum tolerable loads for steady state derived from the FEM simulation. The maximum heat flux density is found at the point where either the inner wall temperature reaches 345 °C or the maximum Von Mises stress equals the yield stress (temperature dependent). The limiting factor is indicated in bold text. The CPS thickness is varied such that PFS reaches around 1250°C when the maximum load is applied.

pipe material	$P_{max,steady}$ [MW/m^2]	$T_{pipe,max}$ [°C]	$\sigma_{mises}/\sigma_{y(T)}$ [-]	max. CPS thickness [mm]	$T_{PFS,max}$ [°C]
Densimet 176	**15**	296	limit: 0.98	2.7	1235
W/Cu 85/15	**22.5**	336	limit: 0.99	2	1252
W/Cu 60/40	**25.3**	limit: 345	0.7	1.8	1223
CuCrZr	**26.5**	limit: 345	0.53	1.9	1255

5.4. Resilience against millisecond pulses

Finally, the resilience against millisecond pulsed loads is assessed. Fig. 8 shows the temperature response expected during disruptions and unmitigated ELMs. The imposed pulse has a triangular shape in time, with a peak power density of 80 GW/m^2, lasting 4 ms. The pulses are applied on top of the maximum tolerable steady state load of 21 MW/m^2, for a CuCrZr pipe with 2.5mm thick CPS. the maximum temperature that is achieved is strongly dependent on R and ϵ_{cool}. It plays a role here that the vapor pressure is a less strong function of temperature than it is during steady-state scenarios, due to relatively higher temperatures. The melting temperature of tungsten is taken as a failure criterion. Excursions above the recrystallization temperature are not considered problematic, even though this might weaken the material, because stresses in the CPS are generally low.

Because the effective values of R and ϵ_{cool} cannot be determined precisely, a worst- and a best-case scenario are considered. As in Section 5.2, we can determine that $\epsilon_{cool} = 6000$ eV from [23], by estimating that the electron density during an ELM is at least 10^{21} m^{-3}. Yet, as a worst-case scenario, it is assumed that $\epsilon_{cool} = 600$ eV, and, that only a

Table 2
Maximum tolerable loads for slow transients derived from the FEM simulation for a CuCrZr pipe with different CPS thicknesses. The maximum heat flux density is found at the point where either the heat flux density through the inner wall reaches the CHF of 56.1 MW/m^2 or the maximum Von Mises stress equals the yield stress (temperature dependent). A higher thickness results in higher tolerable power because more power is vapor shielded. For each CPS thickness also the maximum tolerable power in steady state is derived, which decreases with increasing CPS thickness due to overheating of the PFS. *For a 3mm thick CPS, vapor shielding is strong enough to withstand the maximum expected load of 80 MW/m^2, but this is not the maximum possible load.

CPS thickness, t [mm]	off-normal P_{max} **[MW/m^2]**	off-normal $P_{innerwall}$ [°C]	off-normal $\sigma_{mises}/\sigma_{y(T)}$ [-]	vapor shield fraction [-]	steady-state $P_{max,steady}$ [MW/m^2]	steady-state $T_{pipe,max}$ [°C]	steady-state $\sigma_{mises}/\sigma_{y(T)}$ [-]	steady-state $T_{PFS,max}$ [°C]
2	**42**	50.5	limit: 1	0.068	**25.5**	341	0.5	limit: 1257
2.5	**57**	50.2	limit: 1	0.323	**21**	315	0.4	limit: 1247
3	**80***	46.6	0.89	0.551	**18**	297	0.35	limit: 1246

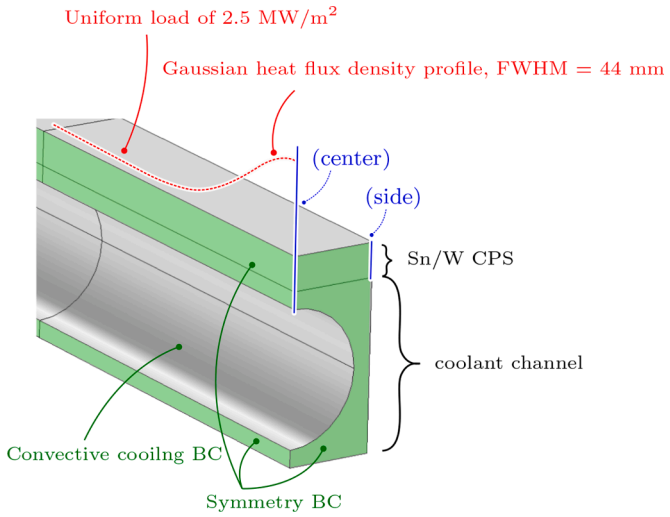

Fig. 5. Setup of the used FEM model. The indications 'center' and 'side' show where the temperature profiles shown in Fig. 7 were taken.

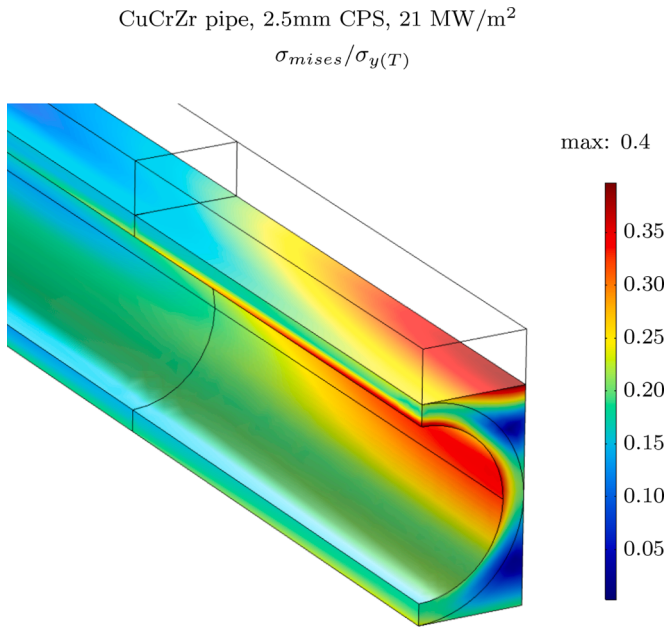

Fig. 6. Von Mises stresses during steady state operation at 60 MW/m^2. The CPS is considered to have no stiffness, and is therefore neglected for this result. Analysis of the individual stress components (not shown) indicated that stresses oriented along the length of the pipe are the main contribution to the Von Mises stress.

fraction $(1-R)$ of the evaporated flux contributes to vapor shielding. In this case the tungsten substrate melts during disruptions when $R \geq 0.9$. When $R = 0.9$ and $\epsilon_{cool} = 6000$ eV, the substrate stays below the melting point. For the best-case scenario we assume that up to 100% of evaporated particles contribute to vapor shielding. This is because ϵ_{cool} may be dissipated mainly in the form of radiation, regardless of whether particles are redeposited or not, which is in fact not unlikely. If 100% of the particles remove 6000 eV, the PFS will not exceed $\sim$ 2250°C. When 50% of the evaporated particles each reduce the incoming power by 600 eV, the surface temperature will be maximum $\sim$ 3000°C. To determine with more certainty whether disruptions can be withstood is unfortunately not possible at this time, as it requires more detailed simulations or dedicated experiments. It is however deemed well within the realm of possibility.

6. CPS geometry and flow stability

6.1. CPS geometry

A prerequisite for the heat loading capabilities estimated above, is that the liquid tin flow through the CPS is stable and homogeneous. The flow is driven by gravity, but, it is also influenced by the magnetic field, electric currents, and the geometry of the CPS. The latter can be controlled to a high degree, due to the use of 3D-printing to fabricate the CPS. To determine a suitable geometry, several candidate geometries were printed out of plastic and tested with water. The stability and flow rate are assessed, and compared to an analytical estimation of the flow rate. The results in this experiment are used to recommend a final geometry, however, further testing is required to fully demonstrate the feasibility of achieving a stable flow.

The geometry that produced the most stable and homogeneous flow is shown in Fig. 9. The geometry consists of an array of blocks that are tapered towards the pipe. When viewing along the pipes, the channels between these blocks are almost triangular. The gap between the blocks is 1.5 mm nominally on the pipe surface, and narrows to $\sim$0.2 mm at the PFS. The PFS itself is flat. No fine texturing could be applied due to insufficient printing resolution for plastic. The height of the test piece is 150 mm. The substrate to which the CPS is attached is printed in the same step, and mimics the geometry of the coolant channels. Including the spaces between the pipes.

The test shows that the water flow is both stable and homogeneous across most of the PFS, see Fig. 10. The only exceptions are the corner, where the CPS is curved, and the region near the inlet at the top, where the flow is still developing. The inlet flow rate is set at the point where the CPS is neither under-filled nor overflowing, which was determined by eye. The velocity of the flow is measured by two approaches. First, the velocity is derived from the inlet flow rate by dividing by the calculated flow area within the CPS. Second, colorant is injected and tracked, as shown in Fig. 10. The two measurements agree well, and result in flow rates of 0.22 ± 0.02 m/s and 0.29 ± 0.07 m/s respectively.

The flow rate is also estimated using a 0-D analytical model. The model assumes that the flow is fully developed, homogeneous, and

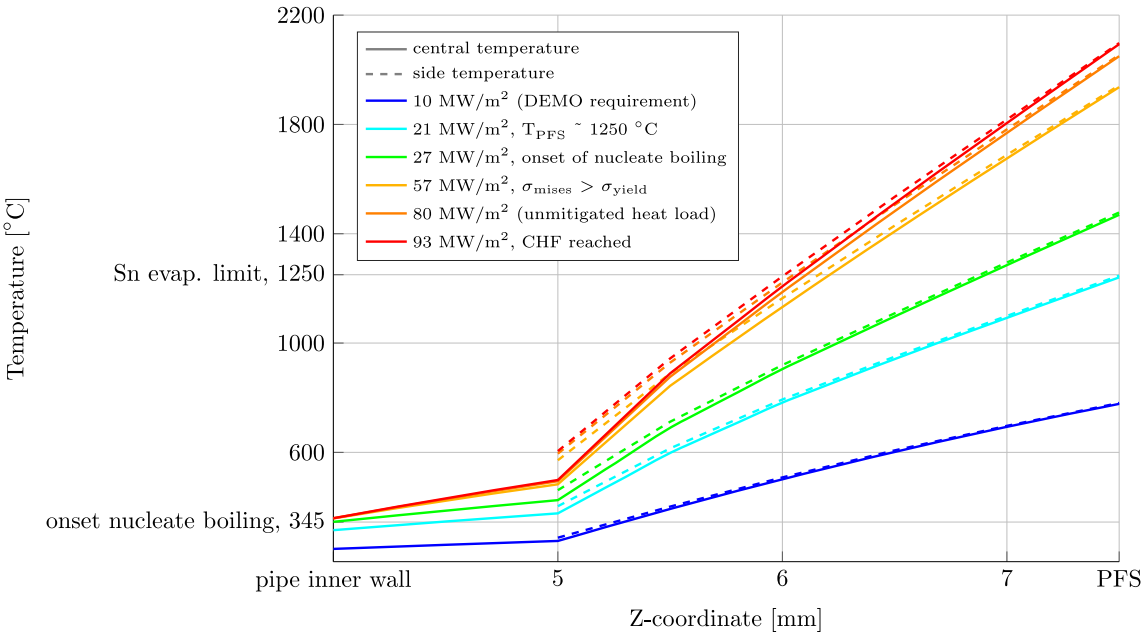

Fig. 7. Vertical temperature profiles ranging from the PFS, down to the pipe surface (5 mm), and to the pipe inner wall 1 mm lower. The profiles are taken in the center of the pipe, and on the side (dashed), as indicated in Fig. 5. At an incoming heat flux density of 23.8 MW/m^2 the onset of nucleate boiling is reached. At an incoming heat flux density of ~ 60 MW/m^2 the CHF of the coolant is reached. Indicated by the black dashed lines are: The temperature for the pipe inner wall where the onset of nucleate boiling occurs (345 °C); The temperature below which the W/Cu has a tensile strength above 500 MPa (816 °C); The temperature below which Sn evaporation is acceptable (1250 °C).

laminar. Bernoulli's equation can in this case be simplified to Eq. 1, where ΔP is the pressure drop across the entire flow path, ρ is the liquid density, h is the height difference between the beginning and end of the flow path, and g is the gravitational acceleration. The pressure drop across the CPS is given in Eq. 2. The first term describes the viscous friction for trapezoidal channels as described in [49]. The second term describes the MHD drag caused by the magnetic field. Here, μ is the viscosity, v is the flow velocity, D_h is the hydraulic diameter, B is the strength of the B-field, σ is the electrical conductivity of the liquid, and L is the length of the flow path. Po is Poiseuille number as determined in [49]. For the flow test with water and a plastic CPS, the MHD drag is not applicable because no magnetic field was used. For this case a flow rate of 0.53 m/s was found, which is on the same order of magnitude as the experimentally determined values.

$$\Delta P = \rho g h \tag{1}$$

$$\Delta P = \left(2\mu v Po / D_h^2 + vB^2\sigma\right)L \tag{2}$$

Coming back to the actual LMD design, where the CPS will be printed from tungsten: it is recommended to use a similar geometry as the one proposed here because of the observed flow stability. Slight changes must be made though. First of all, a texture must be applied to the PFS to prevent droplet ejection, similar to the texture from [18]. Second, to prevent splashing also the channels in between the rectangular structures must be much narrower than in the plastic version, preferably $< 50\ \mu m$. Third, to relieve thermal stresses in the CPS and to create more channels connecting the PFS with the underlying tin flow, it should be considered split the tapered blocks in the structure (fig. 9, to form branches. Again similar to [18].

All these changes to the geometry are not expected to influence the velocity of the tin flow greatly. Rather, it is expected that the presence of the magnetic field will completely dominate the resulting flow rate. For a magnetic field of 1 T, a flow rate of only $8{\cdot}10^{-3}$ m/s is expected. For DEMO, where the magnetic field can be rougly estimated at 10 T (~5.5 T on axis and ~12 T on the conductors [50]), this value is reduced to $8{\cdot}10^{-5}$ m/s. This velocity corresponds to a total flow rate through the divertor of about $1.2{\cdot}10^{-2}$ L/s, which is considered suitable. Namely, at such a low flow rate the pumping power, required to recirculate the LM from the CPS outlet to the inlet, is expected to be acceptable (the flow through the CPS itself is gravity driven). Furthermore, the flow rate is still various orders larger than the total expected evaporation flux, which is estimated at $3.8{\cdot}10^{-6}$ L/s in the 26.5 MW/m^2 steady state case from Table 1, and thus the CPS should not dry out.

7. Discussion

A conceptual LMD design is proposed, that can meet all requirements. Excessive tritium retention is avoided by the use of tin. This also means that the divertor is a high recycling surface for hydrogen, as required. Though tin does activate slightly, sufficiently little is used so that waste and safety limits are not exceeded. Surface temperatures are kept below the limit for excessive evaporation during steady state. The gravity driven flow across the surface allows the target to be the required height, and also allows for forces re-wetting in case of accidental dry out. The divertor can be exposed to atmosphere during maintenance without excessive oxidation of the tin. Only the heat loading capability depends on the materials used for the cooling channels.

FEM analysis shows that all materials are able to meet the steady-state heat load requirement of 10 MW/m^2, or even significantly exceed it, even if a safety factor of 1.4 is applied. In the best case, When CuCrZr is used, 26.5 WM/m^2 can be tolerated in steady-state, when the CPS is thinner than 1.9 mm. When the CPS thickness is increased, the resilience to slow transients goes up. A CPS of 3 mm thick on a CuCrZr pipe would allow slow transients in excess of 80 MW/m^2, while the steady-state load goes down to 18 MW/m^2 (13 MW/m^2 taking the safety factor into account). The requirement for slow transients of maximum 21 MW/m^2 cannot be met when Densimet 176 or W/Cu 85/15 is used. These materials have too low thermal conductivity and too high stiffness, causing the yield stress to be exceeded during slow transients.

Note, however, that the final material choice should not be based solely on the theoretical heat loading capability. The bonding between the cooling channels, corrosion barrier, and 3D-printed CPS is equally

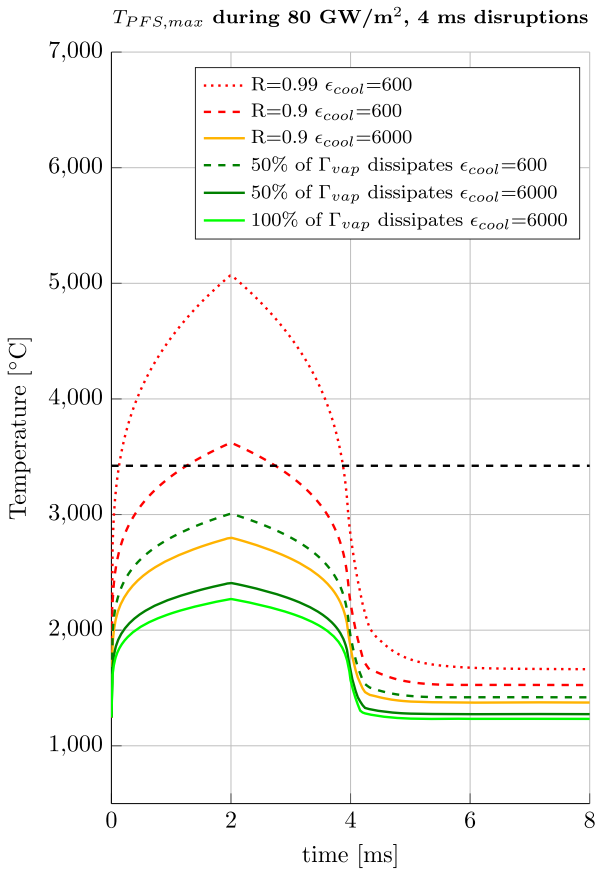

Fig. 8. Temperature evolution during disruptions. Several combinations of R and ϵ_{cool} were considered, as well as the case where a percentage of particles removes ϵ_{cool} from the beam regardless of redeposition. This could be the case when energy is mainly dissipated via radiation. Also the temperature response during ELMs is given (gray), as well as the melting point of tungsten (black dashed). All material properties are kept constant, regardless of temperature. This introduces a negligible error in the temperature because ~99.5% of the incoming power is vapor shielded in all cases.

important, as this determines the lifetime to a large degree. The LM PFS is self healing after all. Additionally, also the lifetime of the corrosion barrier surrounding the pipe is unknown, which is affected by both thermal cycling and liquid metal corrosion. To assess the lifetime of the component is recommended to conducting thermal cycling, and corrosion tests on realistic mock ups of different materials.

Finally, it could not yet be concluded whether disruptive heat loads could be withstood. Experimental tests on CPS targets have shown that disruptive loads can be handled when Li is used [14]. However, tin has a much lower vapor pressure, which makes the tungsten CPS more likely to melt, as the surface temperature required for sufficient vapor shielding to occur is much higher. Nevertheless, the modeling results from Fig. 8 indicate that dependent on the effective values of R and ϵ_{cool}, disruptions could also be tolerated by Sn-filled CPS. It should be noted, however, that the specified heat flux density onto the divertor during disruptions, from Section 2, is based on an estimate for ITER. In the EU-DEMO, an even higher heat flux density should be expected, since the plasma stored energy is increased from ~ 350 MJ in ITER [26] to ~ 1 GJ in the EU-DEMO reactor [51]. This should be carefully taken into account before any definitive statement about the resilience of LMDs against disruptions can be made.

Resilience against disruptions would be perhaps the most significant improvement that can be made using an LMD. Currently the baseline tungsten divertor design is likely to sustain extensive damage during disruptions or even unmitigated ELMs, based on predictions for ITER [52]. This will be worse in DEMO, which may therefore be fragile and economically impractical. It is therefore recommended to experimentally test the resilience of LMDs against disruptions in the near future.

7.1. Future work towards DEMO

Several concrete steps are proposed for future work, apart from the tests suggested directly above. With regards to the proposed CPS geometry: The LM flow scheme is proposed to realize a sufficiently high PFS, as required. In this scheme, the simplest approximation is that the flow is purely driven by gravity. It is expected that the flow though the CPS reaches a constant terminal velocity almost directly at the LM inlet, due to viscous friction in the CPS and due to MHD drag. Flowing at a constant velocity will allow the flow cross section to also remain constant, and thus the liquid should not bulge out of the CPS at any point. This is demonstrated in the water flow experiment from Section 6.

The reality of a fusion reactor, however, will be more complicated: First, the MHD drag must be taken into account; second, heat loading will locally increase the depth of melt layer, and thus change the local flow area (recall that with the 180°C coolant only the top 1 mm of the Sn is liquid outside the strike point); third, plasma loading will induce electric currents which will give rise to $j \times B$ forces in the presence of the magnetic fields. In addition, it must be considered whether it is possible

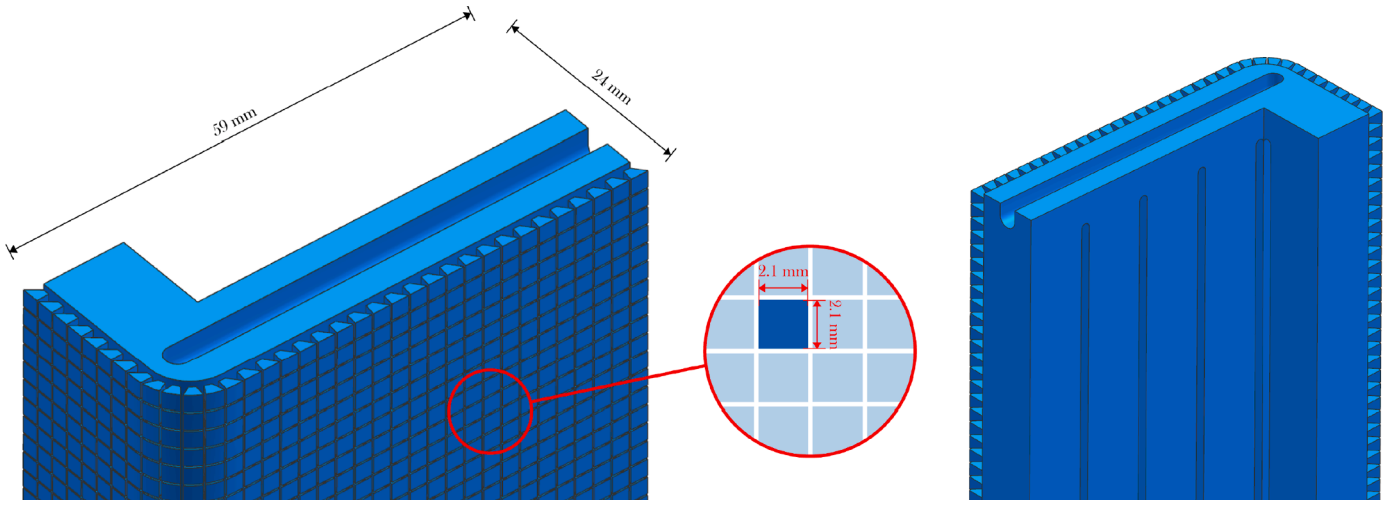

Fig. 9. CAD drawing of the plastic CPS used for the water flow test. The proposed CPS geometry consists of rectangular knobs that are tapered towards the coolant channels. This creates a trapezoidal channel for the liquid metal to flow through from top to bottom.

Fig. 10. Photograph of the water flow experiment in progress. The water flow is homogeneous and stable across most of the surface. Overflowing is only observed where the CPS curves around the corner, and near the water inlet.

for the PFS to have a slight overhang, while maintaining a stable LM flow inside the CPS. Finally, the LM inlet flow must controlled well to closely match the flow through the CPS, which poses a practical challenge. A test in a linear plasma device or experimental tokamak is heavily recommended to assess whether all of these effects and demands can be dealt with. Such a test is essential because the flow behavior, as well as the resilience to thermal cycling will determine the eventual CPS geometry.

Additionally, several essential engineering details should be worked out, which are beyond the scope of this paper: The connection of the coolant channels to inlet and outlet manifolds must be determined. This will be challenging due to the closer packing of cooling channels compared to the monoblocks. The exact geometry of the LM inlet and outlet must be decided. Their geometry must be chosen so that inlet and outlet effects do not result in un-homogeneity's in the LM flow. Finally, the placement of the water and LM manifolds must be considered. These may have to be put in shadowed regions to avoid overheating, while at the same time, freezing of the LM in the manifolds must be avoided.

7.2. Beyond DEMO

Looking beyond DEMO, further improvement of the divertor performance may be required. Higher heat loads may have to be tolerated, as for example in more compact high-field tokamaks, or higher coolant temperatures may be required to enable higher thermodynamic efficiency of the plant. It appears from this design study, however, that this is unfeasible in any LMD design where the incoming heat flux is conducted directly to the coolant. As shown in Table 1 and 2, increasing the incoming heat flux density will cause either overheating of the PFS, or the stresses in the pipe will exceed the yield stress. Moreover, coolants with higher temperature are likely to have lower critical heat fluxes. Therefore the only possible option for further improvement is to spread out the incoming heat flux before it is conducted to the coolant.

Although this paper will not go in detail, two possible ways to achieve this are foreseen: a fast liquid metal flow can be used, or vapor shielding can be used. A fast liquid metal flow has the advantage of creating a cool liquid metal surface, from which evaporation may even be reduced compared to the currently proposed design. The challenge however is to overcome the magnetic drag force. This challenge is substantial, considering that the required flow rate is on the order of 1 m/s [20], which is three orders of magnitude higher than the flow rate expected here. The second option for spreading out the heat flux might be more feasible: vapor shielding inside a vapor box. Vapor shielding has been demonstrated to effectively protect underlying surfaces from severe heat fluxes, including ELM-like pulses [35]. The incoming heat flux is directed elsewhere via radiation and particle transport. The challenge will be to prevent contamination of the plasma by the evaporated tin. In [53] it is proposed to achieve this through the use of a vapor box, but this has not yet been demonstrated. All methods of heat flux spreading have the common advantage that materials may be used with lower thermal conductivity and strength, allowing for the use of materials that activate less than e.g. copper. This could possibly reduce nuclear waste from the divertor.

8. Conclusion

The liquid metal divertor concept proposed in this work is suitable for application in DEMO. In this design liquid tin is used to avoid problematic tritium retention. The tin is confined in a 2 to 3 mm thick 3D-printed tungsten CPS. This CPS is printed on top of a cooling channel, which is round on the inside ($D = 8$ mm) and square on the outside ($w = 10$ mm). This channel is coated in tungsten to prevent corrosion by the tin. Water at 180 °C, 15 MPa, and 14 m/s is used as a coolant. The heat loading capability depends on the material choice for the coolant channels and the CPS thickness. Channels made of CuCrZr allow for the highest heat loading capability. Combined with a 1.9mm thick CPS a maximum steady-state load of 26.5 MW/m can be withstood (18.9 MW/m including safety factor). Increasing the CPS thickness increases the

maximum load during slow transients to more than 80 MW/m, while it reduces the steady state capability to 18.0 MW/m. The final material choice, however, must also take into account the bonding between the coolant channels, corrosion barrier, and CPS. In that aspect Cu/W composites might be favorable, due to more similar thermal expansion coefficients. Compared to the monoblock design, the heat loading capability is generally improved. Resistance against disruptions cannot yet be confirmed with certainty, but is not outside the realm of possibility. Currently, the tungsten monoblock design is not resilient against disruptions, and a single disruption can render the divertor, and thus the entire machine, unusable. In case a liquid Sn divertor is indeed resilient against disruptions, this is considered a major improvement of the robustness of the entire fusion reactor.

Given the predicted performance, it is recommended to develop this concept further. Resilience against disruptions should be further investigated experimentally in the near future. Future studies should also confirm whether the required lifetime of 2 FPY can be achieved. For this, mainly the effectiveness of tungsten as a corrosion barrier against tin, and the resistance of the 3D-printed material against thermal cycling should be investigated.

CRediT authorship contribution statement

P. Rindt: Conceptualization, Methodology, Investigation, Visualization, Writing – original draft, Writing – review & editing, Formal analysis. **J.L. van den Eijnden:** Investigation, Formal analysis. **T.W. Morgan:** Supervision. **N.J. Lopes Cardozo:** Supervision.

Declaration of Competing Interest

The authors declare that they have no known competing financial interests or personal relationships that could have appeared to influence the work reported in this paper.

Acknowlgedgments

This work has been carried out within the framework of the EUROfusion Consortium and has received funding from the Euratom research and training programme 2014–2018 and 2019–2020 under grant agreement No. 633053. The views and opinions expressed herein do not necessarily reflect those of the European Commission.

References

[1] J. You, E. Visca, C. Bachmann, T. Barrett, F. Crescenzi, M. Fursdon, H. Greuner, D. Guilhem, P. Languille, M. Li, S. McIntosh, A. Müller, J. Reiser, M. Richou, M. Rieth, European DEMO divertor target: operational requirements and material-design interface, Nuclear Materials and Energy 9 (2016) 171–176, https://doi.org/10.1016/J.NME.2016.02.005.

[2] J. You, G. Mazzone, E. Visca, C. Bachmann, E. Autissier, T. Barrett, V. Cocilovo, F. Crescenzi, P. Domalapally, D. Dongiovanni, S. Entler, G. Federici, P. Frosi, M. Fursdon, H. Greuner, D. Hancock, D. Marzullo, S. McIntosh, A. Müller, M. Porfiri, G. Ramogida, J. Reiser, M. Richou, M. Rieth, A. Rydzy, R. Villari, V. Widak, Conceptual design studies for the European DEMO divertor: rationale and first results, Fusion Eng. Des. 109–111 (2016) 1598–1603, https://doi.org/10.1016/J.FUSENGDES.2015.11.012.

[3] H. Zohm, F. Träuble, W. Biel, E. Fable, R. Kemp, H. Lux, M. Siccinio, R. Wenninger, A stepladder approach to a tokamak fusion power plant, Nucl. Fusion 57 (8) (2017) 086002, https://doi.org/10.1088/1741-4326/aa739e.

[4] B. Sorbom, J. Ball, T. Palmer, F. Mangiarotti, J. Sierchio, P. Bonoli, C. Kasten, D. Sutherland, H. Barnard, C. Haakonsen, J. Goh, C. Sung, D. Whyte, ARC: A compact, high-field, fusion nuclear science facility and demonstration power plant with demountable magnets, Fusion Eng. Des. 100 (2015) 378–405, https://doi.org/10.1016/J.FUSENGDES.2015.07.008.

[5] EUROfusion, European Research Roadmap to the Realisation of Fusion Energy. Technical Report, 2018.

[6] J.H. You, R. Villari, D. Flammini, D. Marzullo, G. Mazzone, Nuclear loads and nuclear shielding performance of EU DEMO divertor: a comparative neutronics evaluation of two interim design options, Nuclear Materials and Energy 23 (2020) 100745, https://doi.org/10.1016/J.NME.2020.100745.

[7] J.H. You, M. Li, K. Zhang, Structural lifetime assessment for the DEMO divertor targets: design-by-analysis approach and outstanding issues, Fusion Eng. Des. 164 (2021) 112203, https://doi.org/10.1016/J.FUSENGDES.2020.112203.

[8] J.H. You, E. Visca, T. Barrett, B. Böswirth, F. Crescenzi, F. Domptail, G. Dose, M. Fursdon, F. Gallay, H. Greuner, K. Hunger, A. Lukenskas, A.V. Müller, M. Richou, S. Roccella, C. Vorpahl, K. Zhang, High-heat-flux technologies for the European demo divertor targets: state-of-the-art and a review of the latest testing campaign, J. Nucl. Mater. 544 (2021) 152670, https://doi.org/10.1016/J.JNUCMAT.2020.152670.

[9] S. Roccella, G. Dose, R. de Luca, M. Iafrati, A. Mancini, G. Mazzitelli, CPS Based liquid metal divertor target for EU-DEMO, Journal of Fusion Energy 2020 39:6 39 (6) (2020) 462–468, https://doi.org/10.1007/S10894-020-00263-4.

[10] M.A. Jaworski, A. Khodak, R. Kaita, Liquid-metal plasma-facing component research on the national spherical torus experiment, Plasma Phys. Controlled Fusion 55 (12) (2013) 124040, https://doi.org/10.1088/0741-3335/55/12/124040.

[11] S.V. Mirnov, E.A. Azizov, V.A. Evtikhin, V.B. Lazarev, I.E. Lyublinski, A.V. Vertkov, D.Y. Prokhorov, Experiments with lithium limiter on T-11M tokamak and applications of the lithium capillary-pore system in future fusion reactor devices, Plasma Phys. Controlled Fusion 48 (6) (2006) 821–837, https://doi.org/10.1063/1.2405907.

[12] G. Mazzitelli, M. Apicella, D. Frigione, G. Maddaluno, M. Marinucci, C. Mazzotta, V. Pericoli Ridolfini, M. Romanelli, G. Szepesi, O. Tudisco, F. Team, FTU Results with a liquid lithium limiter, Nucl. Fusion 51 (7) (2011) 073006, https://doi.org/10.1088/0029-5515/51/7/073006.

[13] R. Kaita, R. Majeski, R. Doerner, G. Antar, J. Timberlake, J. Spaleta, D. Hoffman, B. Jones, T. Munsat, H. Kugel, G. Taylor, D. Stutman, V. Soukhanovskii, R. Maingi, S. Molesa, P. Efthimion, J. Menard, M. Finkenthal, S. Luckhardt, Surface Treatment of a Lithium Limiter for Spherical Torus Plasma Experiments. Technical Report, Princeton Plasma Physics Laboratory (PPPL), Princeton, NJ, 2001, https://doi.org/10.2172/781477.

[14] I.E. Lyublinski, A.V. Vertkov, V.A. Evtikhin, Application of lithium in systems of fusion reactors. 2. the issues of practical use of lithium in experimental facilities and fusion devices, Plasma Devices Oper. 17 (4) (2009) 265–285, https://doi.org/10.1080/10519990903172364.

[15] G.G. van Eden, T.W. Morgan, D.U.B. Aussems, M.A. van den Berg, K. Bystrov, M.C. M. van de Sanden, Self-Regulated plasma heat flux mitigation due to liquid Sn vapor shielding, Phys. Rev. Lett. 116 (13) (2016) 135002, https://doi.org/10.1103/PhysRevLett.116.135002.

[16] P. Rindt, T. Morgan, M. Jaworski, N.L. Cardozo, Power handling limit of liquid lithium divertor targets, Nucl. Fusion 58 (10) (2018) 104002, https://doi.org/10.1088/1741-4326/AAD290.

[17] P. Rindt, T. Morgan, G. van Eden, M. Jaworski, N.L. Cardozo, Power handling and vapor shielding of pre-filled lithium divertor targets in magnum-PSI, Nucl. Fusion 59 (5) (2019) 056003, https://doi.org/10.1088/1741-4326/AB0560.

[18] P. Rindt, J.M. González, P. Hoogerhuis, P. van den Bosch, M. van Maris, D. Terentyev, C. Yin, M. Wirtz, N.L. Cardozo, J. van Dommelen, T. Morgan, Using 3D-printed tungsten to optimize liquid metal divertor targets for flow and thermal stresses, Nucl. Fusion 59 (5) (2019) 054001, https://doi.org/10.1088/1741-4326/AB0A76.

[19] R. Goldston, A. Hakim, G. Hammett, M. Jaworski, J. Schwartz, Recent advances towards a lithium vapor box divertor, Nuclear Materials and Energy 12 (2017) 1118–1121, https://doi.org/10.1016/J.NME.2017.03.020.

[20] M.A. Jaworski, N.B. Morley, D.N. Ruzic, Thermocapillary and thermoelectric effects in liquid lithium plasma facing components, J. Nucl. Mater. 390–391 (2009) 1055–1058, https://doi.org/10.1016/j.jnucmat.2009.01.255.

[21] D. Ruzic, W. Xu, D. Andruczyk, M. Jaworski, K.R. et Al, X.W. Jaworski M.A.Gray T. K., Antonelli M., Kim J.J., Lau C.Y., Lee M.B., Neumann M.J., R. D.N., S. J.A., M. N. Jaworski M.A., R. D.N., J. M.A., R.D. Surla V., Tung M., Xu W., Andruczyk D., Neumann M., M. D., M.R. Jaworski M.A., Gerhardt S.P., Morley N.B., Abrams T., Kaita R., Kallman J., Kugel H., R. D.N., Lithium metal infused trenches (LiMIT) for heat removal in fusion devices, Nucl. Fusion 51 (10) (2011) 102002, https://doi.org/10.1088/0029-5515/51/10/102002.

[22] T.W. Morgan, P. Rindt, G.G. van Eden, V. Kvon, M.A. Jaworksi, N.J.L. Cardozo, Liquid metals as a divertor plasma-facing material explored using the Pilot-PSI and magnum-PSI linear devices, Plasma Phys. Controlled Fusion 60 (1) (2018) 014025, https://doi.org/10.1088/1361-6587/aa86cd.

[23] M. Poradziński, I. Ivanova-Stanik, G. Pełka, R. Zagórski, Integrated core-SOL-divertor modelling for DEMO with tin divertor, Fusion Eng. Des. 124 (2017) 248–251, https://doi.org/10.1016/J.FUSENGDES.2017.04.131.

[24] J.N. Brooks, Modeling of sputtering erosion/redeposition status and implications for fusion design, Fusion Eng. Des. 60 (4) (2002) 515–526, https://doi.org/10.1016/S0920-3796(02)00007-8.

[25] P. Frosi, Development of load specification and structural integrity report for divertor cassesste EFDA_D_2M5PDL V1.2, Technical Report, EUROfusion.

[26] S. Pestchanyi, R. Pitts, M. Lehnen, Simulation of divertor targets shielding during transients in ITER, Fusion Eng. Des. 109–111 (2016) 141–145, https://doi.org/10.1016/J.FUSENGDES.2016.02.105.

[27] G. Federici, L. Boccaccini, F. Cismondi, M. Gasparotto, Y. Poitevin, I. Ricapito, An overview of the EU breeding blanket design strategy as an integral part of the DEMO design effort, Fusion Eng. Des. 141 (2019) 30–42, https://doi.org/10.1016/J.FUSENGDES.2019.01.141.

[28] C. Day, T. Giegerich, The Direct Internal Recycling concept to simplify the fuel cycle of a fusion power plant. Fusion Engineering and Design 88, North-Holland, 2013, pp. 616–620, https://doi.org/10.1016/j.fusengdes.2013.05.026.

[29] M. Kovari, M. Coleman, I. Cristescu, R. Smith, Tritium resources available for fusion reactors, Nucl. Fusion 58 (2) (2018) 026010, https://doi.org/10.1088/1741-4326/aa9d25.
[30] B. Bornschein, C. Day, D. Demange, T. Pinna, Tritium management and safety issues in ITER and DEMO breeding blankets. Fusion Engineering and Design 88, North-Holland, 2013, pp. 466–471, https://doi.org/10.1016/j.fusengdes.2013.03.032.
[31] S.J. Piet, E.T. Cheng, S. Fetter, J.S. Herring, Initial integration of accident safety, waste management, recycling, effluent, and maintenance considerations for low-Activation materials, Fusion Technol. 19 (1) (1991) 146–161, https://doi.org/10.13182/FST19-1-146.
[32] M. Baldwin, R. Doerner, S. Luckhardt, R. Conn, Deuterium retention in liquid lithium, Nucl. Fusion 42 (11) (2002) 1318–1323, https://doi.org/10.1088/0029-5515/42/11/305.
[33] F. Maviglia, R. Albanese, R. Ambrosino, W. Arter, C. Bachmann, T. Barrett, G. Federici, M. Firdaous, J. Gerardin, M. Kovari, V. Loschiavo, M. Mattei, F. Villone, R. Wenninger, Wall protection strategies for DEMO plasma transients, Fusion Eng. Des. 136 (2018) 410–414, https://doi.org/10.1016/J.FUSENGDES.2018.02.064.
[34] T. Barrett, B. Chuilon, M. Kovari, D. Leon Hernandez, M. Richiusa, E. Rosa Adame, R. Tivey, Z. Vizvary, Y. Xue, F. Maviglia, Designs and technologies for plasma-facing wall protection in EU DEMO, Nucl. Fusion 59 (5) (2019) 056019, https://doi.org/10.1088/1741-4326/ab085b.
[35] P. Rindt. The potential of liquid-metal 3D-printed heat shields for fusion reactors, Eindhoven University of Technology, 2019. Phd thesis.
[36] J. Loureiro, H. Fernandes, F. Tabarés, G. Mazzitelli, C. Silva, R. Gomes, E. Alves, R. Mateus, T. Pereira, H. Figueiredo, H. Alves, Deuterium retention in tin (Sn) and lithium tin (Li Sn) samples exposed to ISTTOK plasmas, Nuclear Materials and Energy 12 (2017) 709–713, https://doi.org/10.1016/J.NME.2016.12.026.
[37] A. Cremona, E. Vassallo, E. Alves, F. Causa, S. De Iuliis, R. Dondè, G. Giacomi, G. Gervasini, G. Granucci, M. Iafrati, G. Maddaluno, R. Mateus, D. Minelli, V. Mellera, A. Nardone, M. Pedroni, D. Ricci, V. Rigato, N. Rispoli, A. Uccello, Deuterium retention and erosion in liquid sn samples exposed to D2 and Ar plasmas in GyM device, Nuclear Materials and Energy 17 (2018) 253–258, https://doi.org/10.1016/j.nme.2018.11.010.
[38] W. Ou, R. Al, J. Vernimmen, S. Brons, P. Rindt, T. Morgan, Deuterium retention in Sn-filled samples exposed to fusion-relevant flux plasmas, Nucl. Fusion 60 (2) (2020) 026008, https://doi.org/10.1088/1741-4326/AB5CD4.
[39] T. Hirai, S. Panayotis, V. Barabash, C. Amzallag, F. Escourbiac, A. Durocher, M. Merola, J. Linke, T. Loewenhoff, G. Pintsuk, M. Wirtz, I. Uytdenhouwen, Use of tungsten material for the ITER divertor, Nuclear Materials and Energy 9 (2016) 616–622, https://doi.org/10.1016/J.NME.2016.07.003.
[40] T. Wegener. Investigations of liquid metals as a first wall materials for fusion reactors at the linear plasma device PSI-2., FH Aachen University of Applied Sciences, 2013. Master thesis.
[41] S. Yin, A. Cardella, A. Abdelmessih, Z. Jin, B. Bromley, Assessment of a heat transfer correlations package for water-cooled plasma-facing components in fusion reactors, Nucl. Eng. Des. 146 (1–3) (1994) 311–323, https://doi.org/10.1016/0029-5493(94)90338-7.
[42] E. Rabaglino, J. Schlosser, F. Escourbiac, M. Merola, B. Panella, Prediction of heat transfer in water actively cooled plasma facing components, 2000.
[43] K. Zhang, E. Gaganidze, M. Gorley, Development of the material property handbook and database of CuCrZr - UKAEA Scientific Publications.
[44] G. Pintsuk, J. Blumm, W. Hohenauer, R.C. Hula, T. Koppitz, S. Lindig, D. Pitzer, M. Rohde, P. Schoderböck, T. Schubert, F. Tietz, O. Wouters, Interlaboratory test on thermophysical properties of the ITER grade heat sink material copper-Chromium-Zirconium, Int J Thermophys 31 (11–12) (2010) 2147–2158, https://doi.org/10.1007/s10765-010-0857-y.
[45] E. Tejado, A.V. Müller, J.H. You, J.Y. Pastor, Evolution of mechanical performance with temperature of W/Cu and W/CuCrZr composites for fusion heat sink applications, Mater. Sci. Eng., A 712 (2018) 738–746, https://doi.org/10.1016/j.msea.2017.12.054.
[46] E. Tejado, A.V. Müller, J.H. You, J.Y. Pastor, The thermo-mechanical behaviour of W-Cu metal matrix composites for fusion heat sink applications: the influence of the Cu content, J. Nucl. Mater. 498 (2018) 468–475, https://doi.org/10.1016/j.jnucmat.2017.08.020.
[47] P. Gmbh, Tungsten heavy alloys.
[48] P. Gmbh, Refractory metals for the foundry industry.
[49] R. Shah, A. London, Laminar flow forced convection in ducts - 1st edition, 1st, Academic Press, 1978.
[50] G. Federici, W. Biel, M. Gilbert, R. Kemp, N. Taylor, R. Wenninger, European DEMO design strategy and consequences for materials, Nucl. Fusion 57 (9) (2017) 092002, https://doi.org/10.1088/1741-4326/57/9/092002.
[51] R. Wenninger, F. Arbeiter, J. Aubert, L. Aho-Mantila, R. Albanese, R. Ambrosino, C. Angioni, J.-F. Artaud, M. Bernert, E. Fable, A. Fasoli, G. Federici, J. Garcia, G. Giruzzi, F. Jenko, P. Maget, M. Mattei, F. Maviglia, E. Poli, G. Ramogida, C. Reux, M. Schneider, B. Sieglin, F. Villone, M. Wischmeier, H. Zohm, Advances in the physics basis for the European DEMO design, Nucl. Fusion 55 (6) (2015) 063003, https://doi.org/10.1088/0029-5515/55/6/063003.
[52] R.A. Pitts, X. Bonnin, F. Escourbiac, H. Frerichs, J.P. Gunn, T. Hirai, A.S. Kukushkin, E. Kaveeva, M.A. Miller, D. Moulton, V. Rozhansky, I. Senichenkov, E. Sytova, O. Schmitz, P.C. Stangeby, G. De Temmerman, I. Veselova, S. Wiesen, Physics basis for the first ITER tungsten divertor, 2019. 10.1016/j.nme.2019.100696.
[53] R.J. Goldston, R. Myers, J. Schwartz, The lithium vapor box divertor, Phys. Scr. T167 (T167) (2016) 014017, https://doi.org/10.1088/0031-8949/T167/1/014017.